Anomaly Detection and Prognosis for Primary Flight Control EMAs

Andrea De Martin[1], Giovanni Jacazio[2], and George Vachtsevanos[3]

[1,2]*Politecnico di Torino, Torino, 10129, Italy.*
andrea.demartin@polito.it
giovanni.jacazio@polito.it

[3]*Georgia Institute of Technology, Atlanta, GA, 30332, USA*
gjv@ece.gatech.edu

ABSTRACT

One of the most significant research trends in the aeronautic industry is currently the design and, possibly, build of "more electric aircraft". In this framework, one of the more deeply investigated subjects has been, and still is, the replacement of the traditional hydraulic/electro-hydraulic technology for flight control systems with the electro-mechanical ones. Although featuring many advantages, electro-mechanical actuators still suffer from several shortcomings, mainly those related to reliability issues, which are still difficult to overcome simply by design. The development of an efficient PHM system could instead provide the needed increase in reliability without any major design variations. This paper addresses, in the first part of the study, the design of a comprehensive PHM system for EMAs employed as primary flight control devices; the peculiarities of the application are presented and discussed, while a novel approach based on short pre-flight health tests is proposed. The most common electric motor windings degradation is addressed in the second part and a particle-filtering framework for anomaly detection and prognosis is proposed featuring a self-tuning non-linear model for improved prognostic performance. Features, anomaly detection and the prognostic algorithm are hence evaluated through state-of-the art performance metrics and their results discussed.

1. INTRODUCTION

Following the last development of the aviation industry, electro-mechanical actuators (EMAs) are slowly replacing the traditional electro-hydraulic solution for fly-by-wire flight controls since they allow the elimination of leaking problems, simplification of installation and maintenance while keeping an overall competitive weight (Pratt, 2000). However, due to reliability problems, they are still struggling to find application outside experimental aircraft or UAVs like reported by (Jensen, Jenney & Dawson, 2000), (Derrien, Tieys, Senegas & Todeschi, 2011), (Roemer & Tang, 2015). They are instead more rapidly advancing in non-safe critical applications such as flap/slats control as described in (Christmann M., Seemann S. & Janker, 2010) and (Recksieck, 2012). In order to overcome the afore-mentioned reliability issues, one of the possible solutions is to build an efficient PHM system able to rapidly detect the insurgence of dangerous fault conditions and to provide a sufficiently accurate assessment of the Remaining Useful Life (RUL) of the degraded component(s). Several research efforts can be found in the literature, addressing the electric motor (Nandi, Toliyat.& Li, 2005), (Brown and others, 2009), and (Belmonte, Dalla Vedova & Maggiore, 2015), mechanical components (Balaban, Saxena, Goebel, Byington, Watson and others, 2009), (Balaban, Saxena, Narasimhan, Roychoudhury & Gobel, 2010) and (Lessmeier, Enge-Rosenblatt, Bayer & Zimmes, 2014) and electronic power unit (EPU) (Brown, Abbas, Ginart, Ali, Kalgren, Vachtsevanos, 2010), (Li, Ye, Chen, Vachtsevanos, 2014).

The research presented in this work introduces the modelling framework and the enabling technologies for a rigorous data mining, diagnostic and prognostic approach to the EMA problem and constitutes the first part of a wider programme aiming to build, test and evaluate a complete PHM system for a primary flight control application. Research and experimental studies addressed aspects of component modelling, feature extraction and diagnostics/prognostics for EMA systems.

2. EMA CONFIGURATION

The system configuration used for the analysis is depicted in Figure 1. Following the most frequent architecture for electro-mechanical flight control units, each actuator

features a brushless electric motor (EM) supplied through its own EPU and a mechanical transmission composed by a satellite gearbox (GB) and a roller screw. Control of each actuator is performed by three nested regulation loops working on the electric motor currents, driving shaft speed and end-user linear position. Feedback signals come respectively from current sensors, a resolver positioned on the motor shaft and a linear position sensor, usually one or more LVDTs, connected to the translating element of the power screw. The position command is provided by two inter-communicating Flight Control Computers (FCCs). The control is performed following the active/active strategy, which means that both devices are contemporary actuated in position receiving the same command input. This control strategy allows to obtain better dynamics response and/or to decrease the intensity of the current required by the motors, but suffers from force fighting occurrence. When this happens, one of the actuators begins to provide a force which sign is the opposite of what is expected under normal operations, hence requiring the other device to compensate. This phenomenon usually happens when the aerodynamic load acting on the system is a small percentage of the nominal one and it's due to the inevitable deviation from the nominal value of some of the actuators features such as friction behaviour, backlashes, inertia and motor parameters. It may lead to windings overheating and generally shortens the motor operative life. Force fighting can be compensated by motor current equalization or, if possible, by monitoring the force applied to each actuator using the proper transducers: their signal, properly filtered and sampled, can then be employed by a dedicated PI controller working either on the position or the speed loop (Wang, Maré, Fu, 2012). For the studied system, force sensors are supposed to be available.
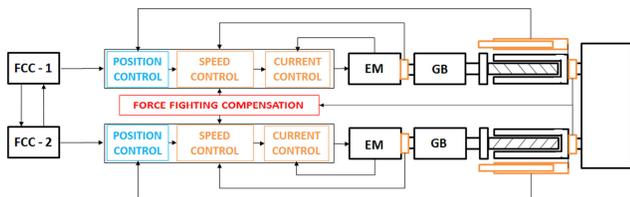
Figure 1. EMA configuration

3. FMECA

Electro-mechanical actuators can be subjected to a high number of possible failure modes, involving both the hardware components, that is the focus of this research, and the control software. In order to have a more precise idea of which failure modes needs to be prioritized, a FMECA study is recommended (Vachtsevanos, Lewis., Roemer, Hess, Wu, 2006). The first step is to establish the FMECA rules set, that is to associate a score to each possible operating occurrence regarding the fault frequency (F), severity (S), testability (T) and failure related replaceability

(R). Each parameter has been ranked from 1 (worst case scenario) to 4 (best case). In example, a frequent fault of high severity and little testability/replaceability will score (F) = 1, (S) = 1, (T) = 1, (R) = 1, leading to an overall minimum of 4 points. Results of the FMECA study are described in table 1. Looking at the severity, the most critical failure modes for the system are those involving an increase in the jamming probability, which is directly associated with the aircraft loss and critical danger for the passengers' life. The interested components are all parts of the mechanical transmission. The most frequent failure mode affects instead the electrical part of the actuation system: the turn-to-turn short failure mode (EMTTS) is in fact the most common degradation for brushless motors and according to (Nandi and others, 2005) is often the primary cause for the inception of other electrical faults that lead to the motor loss as well. Contrary to mechanical failures that may cause the actuator(s) jamming, motor failure is not directly related to flight control loss, even if it causes a significant degradation in the system performance. Although there are some failure modes which total score is equal or inferior to the one associated with EMTTS case, its high frequency and overall low score suggest to use it as the starting point for the study of a PHM framework for the entire actuation system.

Table 1. FMECA results

COMPONENT	MAIN FAILURE MODES	SCORE				
		F	S	T	R	TOT
EPU	Power MOSFET thermal failure	3	2	4	1	10
Electric motor	Turn-to-turn short	1	2	4	1	8
	Turn-to-phase short	2	2	4	1	9
	Turn-to-ground short	2	2	4	1	9
Bearings	Scoring	3	1	3	1	8
	Indentation	4	1	3	1	9
	Wear	4	4	3	1	12
	Pitting	4	4	3	1	12
	Electric erosion	3	2	3	1	9
	Tracks crack	3	1	3	1	8
Gears	Crack	3	1	3	1	8
	Wear	4	4	4	1	13
	Pitting	2	3	3	1	9
Power screw	Scoring	2	1	3	1	7
	Wear	3	4	4	1	12
	Return channel deformation	4	1	3	1	9
	Indentation	3	1	3	1	8

4. EMA DYNAMIC MODEL

A high-fidelity dynamic model built in Matlab Simulink has been used to simulate the system under several operating

2

conditions in order to obtain realistic data for the PHM system.

4.1. EPU and brushless motor model

The dynamic model of the electric actuation is composed by several interconnected functional subsystems: the EPU, the motor windings and the torque evaluation module. The EPU subsystem is used to simulate the control currents in d-q axis, the PWM modulation of the voltage signal and a functional model of the digital inverter. The other subsystems describe the electric motor dynamics for each phase, compute the electromagnetic torque and approximate the windings thermal behavior. The d-q axis control features PI regulators receiving as input the current command and the filtered current feedback subjected to Park transformation. The controllers' output is then transformed back to the three-phase system and used in a PWM modulator based on a triangular bipolar wave carrier that generates the vector of the digital control signal for each of the three commutation poles, namely $\boldsymbol{q} = [q_1 \ q_2 \ q_3]^\mathrm{T}$.

Neglecting the power MOSFET dynamics and modelling the EPU following the approach proposed in (Mohan, 2003) and (Hanselman, 2006), we compute the three motor phase voltages. The motor dynamics under nominal conditions is described by equation (1).

$$\begin{bmatrix} v_a \\ v_b \\ v_c \end{bmatrix} - \frac{d}{dt}\begin{bmatrix} \lambda_a \\ \lambda_b \\ \lambda_c \end{bmatrix} = \begin{bmatrix} R_a & 0 & 0 \\ 0 & R_b & 0 \\ 0 & 0 & R_c \end{bmatrix}\begin{bmatrix} i_a \\ i_b \\ i_c \end{bmatrix} + \frac{d}{dt}\left(\begin{bmatrix} L_{aa} & L_{ab} & L_{ac} \\ L_{ab} & L_{bb} & L_{bc} \\ L_{ac} & L_{bc} & L_{cc} \end{bmatrix}\begin{bmatrix} i_a \\ i_b \\ i_c \end{bmatrix}\right) \quad (1)$$

Where the three phase voltages $v_{a,b,c}$ are function of $\boldsymbol{q}$. R_i and L_i are the electric resistance and inductance for the i-th phase, while λ_i is the concatenated flux.

Given the pair poles number, the electromagnetic torque can be obtained. It is finally possible to estimate the windings thermal behavior:

$$\begin{bmatrix} i_a \\ i_b \\ i_c \end{bmatrix}^T \begin{bmatrix} R_a & 0 & 0 \\ 0 & R_b & 0 \\ 0 & 0 & R_c \end{bmatrix}\begin{bmatrix} i_a \\ i_b \\ i_c \end{bmatrix} - H_{th}\vartheta_{th} = C_{th}\frac{d\vartheta_{th}}{dt} \quad (2)$$

Where $\boldsymbol{\vartheta_{th}} = \boldsymbol{T_{em}} - \boldsymbol{T_{ext}}$ is the temperature difference between the motor windings and the external environment, while H_{th} and C_{th} are the thermal conductivity and the thermal capacity.

4.2. Mechanical transmission

The mechanical transmission has been modelled to include a non-linear friction law and a customizable elasto-backlash following the approach proposed by (Nordin, Gallic, Gutman, 1997). Each mechanical element is described through its dynamic equilibrium equation. The friction law has been approximated through non-linear equations depending on temperature, speed and applied load.

4.3. Control surface model

The aerodynamic surface has been modelled according to the diagram shown in Figure 2. The dynamic equilibrium of

this component can then be expressed through equation (3):

$$k_s(x_1 - y) + k_s(x_2 - y) + c_s(\dot{x}_1 - \dot{y}) + c_s(\dot{x}_2 - \dot{y}) - F_A = m_s\ddot{y} \quad (3)$$

Where k_s and c_s are the aerodynamic surface stiffness and damping factor, respectively, FA is the aerodynamic force acting on the actuators and m_s the control surface equivalent mass.
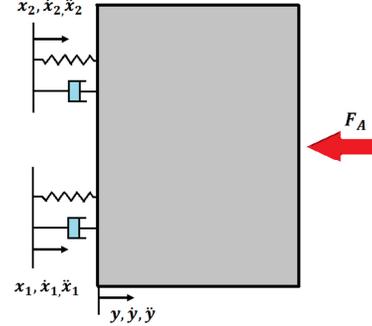
Figure 2. Control surface scheme

4.4. TTS fault model

According to (Brown and others, 2009), it is possible to model the presence of a turn-to-turn short in one of the motor phases by inserting the fault ratio factor w_f in the electrical dynamic equation thus modifying the motor circuit. This parameter may range between 0 and 1 and represents the ratio between the number of healthy windings over the total number of windings for the selected phase.

The phase voltage equations may be written as:

$$\begin{bmatrix} v_a \\ v_b \\ v_c \end{bmatrix} - \frac{d}{dt}\begin{bmatrix} w_{f,a} \\ w_{f,b} \\ w_{f,c} \end{bmatrix}\lambda = \begin{bmatrix} w_{f,a} \\ w_{f,b} \\ w_{f,c} \end{bmatrix}^T \mathbf{R}\begin{bmatrix} i_a \\ i_b \\ i_c \end{bmatrix} + \frac{d}{dt}\left(\mathbf{L_F}\begin{bmatrix} i_a \\ i_b \\ i_c \end{bmatrix}\right) \quad (4)$$

Where $\mathbf{R}$ is the resistance matrix for the healthy state, $\boldsymbol{\lambda}$ is the magnetic flux vector and $\mathbf{L_F}$ is the inductance matrix for degraded conditions defined in equation (5).

$$\mathbf{L_F} = \begin{bmatrix} w_{f,b}L_{aa} & w_{f,ab}L_{ab} & w_{f,ac}L_{ac} \\ w_{f,ab}L_{ab} & w_{f,b}L_{bb} & w_{f,bc}L_{bc} \\ w_{f,ac}L_{ac} & w_{f,bc}L_{bc} & w_{f,c}L_{cc} \end{bmatrix} \quad (5)$$

Where $w_{f,ij} = \sqrt{w_{f,i}w_{f,j}}$ and the variables follow standard notation. The reciprocal index $W_f = 1-w_f$ represents the number of faulted windings over the total number of windings for the phase under analysis.

The effects of the fault progression on the phase currents can be seen in Figure 3. The faulted winding signal tends to increase leading to a current asymmetry and torque irregularity. Through Fourier analysis, it is also possible to notice how the degraded phase current tends to be more distorted as the fault progresses, as depicted in Figure 4.

Turn-to-turn degradation can be triggered and driven by several causes, such as mechanical stresses, chemical aggressive environment, water ingress or excessive humidity (Nandi and others, 2005).

According to (Brown and others, 2009), the most significant and common origin is the insulant's thermal degradation;

3

the same authors report that it is possible to relate the fault length L expressed in [mm] as a function of the operating time t, the windings' temperature T_w and the experimental coefficients α and β through an elaboration of the Arrhenius law (Gokdere, Bogdanov, Chiu, Keller & Vian, 2006):
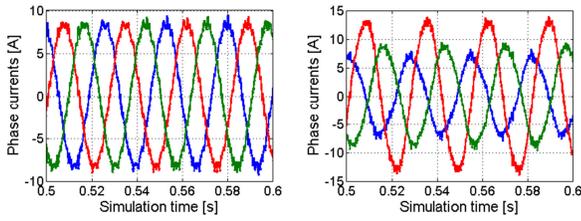
Figure 3. Effect of fault progression on phase currents: healthy (left) severe degradation (right)

$$\begin{cases} L = L_0 e^{\gamma t} \\ \gamma = \beta e^{\alpha T_w} \end{cases} \qquad (6)$$

Dividing the first equation of expression (6) by the critical length of the defect, we obtain a similar relation for the fault rate

$$\begin{cases} W_f = W_{f,0} e^{\gamma t} \\ \gamma = \beta e^{\alpha T_w} \end{cases} \qquad (7)$$

Where $Wf = 1\text{-}wf$ and $W_{f,0}$ are the instantaneous and initial fault rate in the degraded phase.
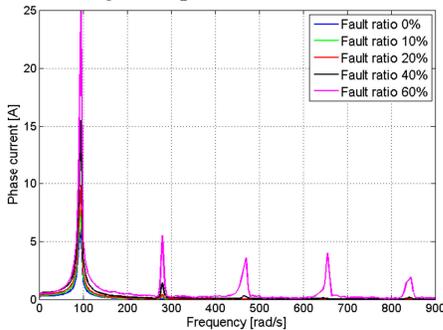
Figure 4. Fourier analysis of the faulted phase current

5. PHM STRATEGY

A rigorous and reliable PHM system requires a set of features or Condition Indicators (CIs) that characterize the fault mode and correlate maximally with the fault signature in a reduced dimensionality. For the turn-to-turn short fault several possibilities are available in the literature (Nandi and others, 2005). Some of them make use of current analysis, while others require the phase voltage measure. Since voltage measures are not available in the case under analysis, current-based features have to be employed.

In order to overcome the effects of uncertainties due to environmental conditions, but also to simulate the actuators with a predefined set of commands optimized to extract the required features, we employ a preflight test according to the approach proposed by (Jacazio, Maggiore, Della Vedova, Sorli M., 2010). In this case, a ramp position command, with rate equal to 20% of the motor maximum speed, is given to the "monitored" actuator, in order to limit the influence of the back electromotive force over the measured current. The second actuator is force controlled, taking advantage of the force sensors already present for the force-fighting compensation. The adopted approach allows to reduce the influence of friction over the force exerted by the second actuator. The commanded force is a ramp saturated at 40% of the nominal value that is high enough to enhance the current analysis while remaining far enough from saturation conditions. The last factor of uncertainty coming from the external environment is the random aerodynamic load that could affect the system under test due to gusts at the airport track. In order to limit its influence, a simple proportional compensator operating on the current regulation of the force-controlled actuator is employed. As shown in Figure 5, without compensation, the external load is in an equilibrium state acted by the "monitored" actuator, hence affecting the behavior of its currents; while the compensator is in use, the disturbance is addressed entirely by the second EMA.

The pre-flight test is 1 second long, while data is acquired over the last 0.5 s. Once completed, the operation is repeated inverting the role of the two actuators. Operational scenario

The TTS fault rate is mainly dependent on the temperature of the windings, implying that it is dependent on the ambient environmental temperature, as well as on the load profile faced by the actuator and on the thermal exchange conditions. Moreover, these conditions may vary depending on the aircraft class, take-off/landing areas and weather conditions. The aircraft class for this study has been identified as the regional transport one, designated for mid-short range travel. Each mission segment conditions, namely pre-flight, take-off, cruise, landing and post-flight, are approximated as follows: starting and arrival point temperatures are drawn from a uniform distribution ranging between -40 and 40. The external temperature at cruise regime is considered equal to -54°C; its variation during landing and take-off is approximated with a linear law. For each flight segment, external loads are estimated through a realistic variable percentage of the nominal force affected by Gaussian noise

6. ANOMALY DETECTION

Fault diagnosis is the first step in the design of a health-based prognostics and health management strategy. It involves three main tasks: fault detection is the process through which the system recognizes any anomalous occurrence, fault isolation, addressing the identity of the damaged component, and finally identification, that leads to the assessment of the fault's severity (Vachtsevanos and others, 2006). Since this paper deals with a single-fault scenario, only the first task is described in the sequel. In the proposed approach, fault diagnosis minimizes the false
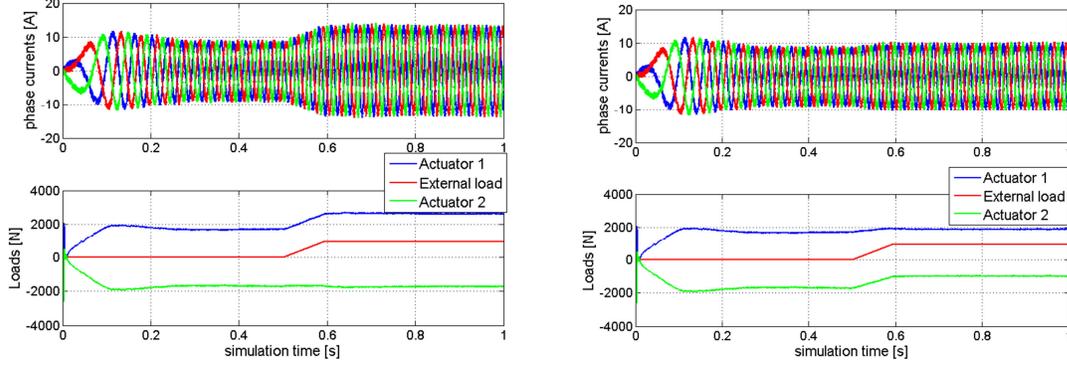
Figure 5. Effect of force compensator: no compensation (left), compensation (right)

positive and false negative errors while providing early defect detection. Anomaly detection is carried out via the application of two approaches: a purely data-driven method and a particle filter framework. The addressed feature candidates are described in section 6.1, where they have been analyzed and compared through proper metrics. In section 6.2 the data-driven approach for anomaly detection is discussed, while a particle filter solution is provided in section 6.3.

6.1. Feature selection

As assessed in section 3, the main effect of TTS degradation is the progressive worsening of currents unbalance. Consequently, features for this failure mode should be able to efficiently mirror this symptom. Three features have been preliminary selected by combining in different ways the RMS of the three currents signals:

$$\begin{cases} f_i^1 = \dfrac{1}{3}\sum_{i=1}^{3} \text{RMS}_i \\ f_i^2 = \dfrac{1}{3}\sum_{i=1}^{3} \Delta\text{RMS}(i) \\ f_i^3 = \max(\Delta\text{RMS}) - \min(\Delta\text{RMS}) \end{cases} \tag{8}$$

Where RMS_i and ΔRMS_i are respectively:

$$\text{RMS}_i = \sqrt{\frac{1}{n_s}\sum_{j=1}^{n_s} i_j{}^2} \tag{9}$$

$$\Delta\text{RMS} = \begin{bmatrix} |\text{RMS}_1 - \text{RMS}_2| \\ |\text{RMS}_1 - \text{RMS}_3| \\ |\text{RMS}_2 - \text{RMS}_3| \end{bmatrix} \tag{10}$$

The current samples number is n_s, while each of their values is designated as i_j. Each feature behavior has been preliminary investigated by performing several simulations at a constant environmental temperature of 0°C without any external load applied. Observing the results reported in

Figure 6, it is noted that each feature candidate presents a clear dependence on the degradation rate W_f. Additional simulations were run in the presence of external disturbances, parameter variations while the external load was simulated as a step signal occurring in a random moment during the pre-flight test.

Features performance are hence analysed through two specific metrics. The first is the accuracy measure, defined as the linear correlation between the feature candidates and the fault ratio. The second one is the precision measure, defined as the relative mean error of the interpolation lines used for each feature candidate.
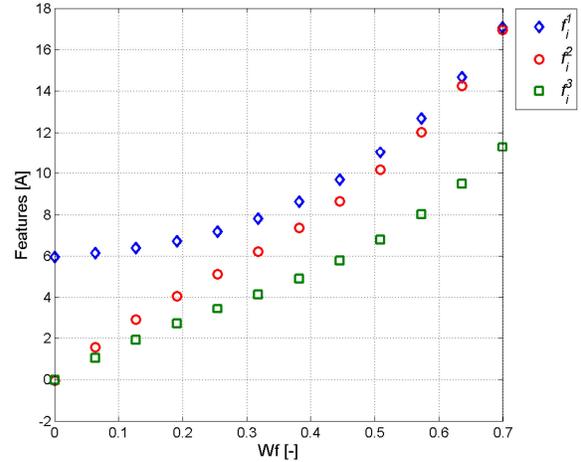
Figure 6 – Feature candidates behaviour – no disturbance

The candidate f_i^1 has better performance, averaging an accuracy index equal to 0.932 and a precision measure of 3.94%. For the other two candidates, the accuracy measure is of 0.925 and 0.921, while the precision one is 9.82% and 9.03% respectively.

6.2. Data-driven approach

A statistical deviation method is adopted for anomaly detection. A baseline representing the feature behavior under healthy conditions is built upon the first 100 samples

of data. An automatic, customizable threshold is set on the feature value covering 95% of the baseline probability distribution. New data are then streaming in and the computed feature is   compared to the initial baseline; when the new distribution differs from the baseline with a specified confidence level equal to or superior to 95%, the fault is declared as having been detected. After repeated trials, feature f_i^1 gives a better mean detection time, while providing more stable performance in response to parameter variations and external disturbances, as shown in Figure 7. The average fault ratio at detection for the selected feature is 12.71%.

An example of the anomaly detection algorithm output making use of the chosen feature f_i^1 is provided in Figure 8. The Type I error is defined by the user and it is fixed at 5%; the Type II error under these conditions has a value of 5%.
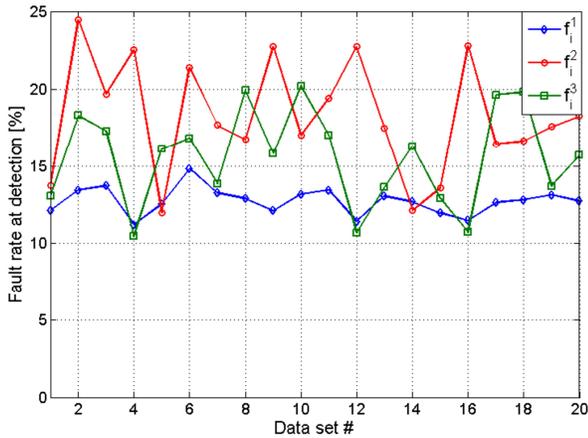
Figure 7. Fault detection for different features candidates
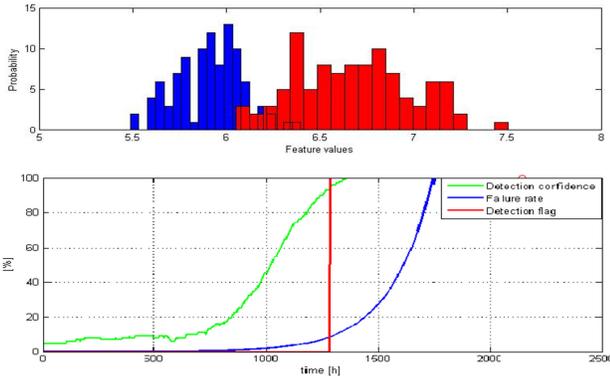
Figure 8. Fault detection framework output

6.3. Particle filter for anomaly detection

Particle filter is a powerful Bayesian estimator that allows to approximate non-linear processes affected by non-Gaussian noise and is recognized as the current state of the art for prognostics (Arulampalam, Maskell, Gordon, Clapp, 2002). The particle-filter-based diagnosis framework aims to

perform the anomaly detection, under general assumptions of non-Gaussian noise structures and nonlinearities in process dynamic models, using a reduced particle population to represent the state pdf (Orchard M, 2007). A compromise between model-based and data-driven techniques is accomplished by the use of a particle filter-based module built upon the nonlinear dynamic state model,

$$\begin{cases} x_d(t+1) = f_b\big(x_d(t), n(t)\big) \\ x_c(t+1) = f_t\big(x_d(t), x_c(t), \omega(t)\big) \\ f_p\ (t) = h_t\big(x_d(t), x_c(t), v(t)\big) \end{cases} \quad (11)$$

Where f_b, f_t and h_t are non-linear mappings, x_d is a collection of Boolean states associated with the presence of a particular operating condition in the system (normal operation, fault type #1, #2, etc.), x_c is a set of continuous-valued states that describe the evolution of the system given those operating conditions, f_p is a feature measurement, ω and v are non-Gaussian distributions that characterize the process and feature noise signals, respectively. The function h_t is a mapping between the feature value, $f_p(t)$, and the fault state $x_c(t)$. At any given instant of time, this framework provides estimates of fault detection only when customer specified confidence and false alarm metrics are met. Furthermore, pdf estimates for the system continuous-valued states may be used as initial conditions in failure prognosis resulting in a swift transition between the two modules (FDI and prognosis).

This approach has been employed only for the selected feature f_i^1. The f_t expression is derived from theoretical considerations while the h_t mapping has been investigated through symbolic regression, leading to the polynomial expression (12).

$$f_i^1 = aw_f^3 + bw_f^2 + cw_f\ + d \quad (12)$$

For non-disturbed data, the R^2 is 0.9983, the mean squared error is 0.027 and the mean absolute error is 1.052. The average fault ratio associated with the detection time, computed over 20 data sets, is reduced to 10.48% while using the same percentage thresholds applied to the data-driven case, indicating superior performance of the algorithm used.

7. PROGNOSTIC FRAMEWORK

Once an incipient failure or fault is detected with specified confidence, the prognostic algorithm is initiated to predict the fault's time evolution. The final fault state acts as the initial condition for prognosis. We pursue a health-based approach to prognosis in this paper. A usage-based approach is useful in reliability studies with prognostic information. Figure 9 depicts the prognostic framework.
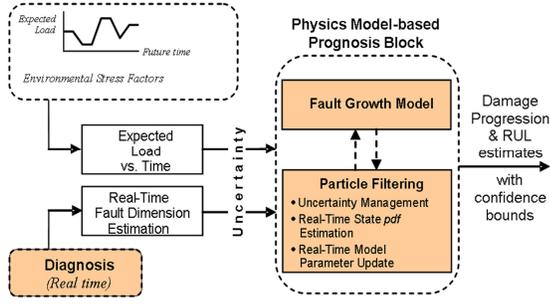
Figure 9. The Prognostic Framework

7.1. Particle filter for failure prognosis

The prognostic framework takes advantage of a nonlinear process (fault / degradation) model, a Bayesian estimation method using particle filtering and real-time measurements (Vachtsevanos and other, 2006). Prognosis is achieved by performing two sequential steps, prediction and filtering. Prediction uses both the knowledge of the previous state estimate and the process model to generate the a priori state pdf estimate for the next time instant,

$$p(x_{0:t}|y_{1:t-1}) = \int p(x_t|y_{t-1})p(x_{0:t-1}|y_{1:t-1}) \, dx_{0:t-1} \qquad (13)$$

Unfortunately, this expression does not have an analytical solution in most cases. Instead, Sequential Monte Carlo (SMC) algorithms, or particle filters, are used to numerically solve this equation in real-time with efficient sampling strategies. Particle filtering approximates the state pdf using samples or "particles" having associated discrete probability masses ("weights") as,

$$p(x_t|y_{1:t}) \approx \widetilde{w}_t\big(x^i_{0:t}\big)\delta\big(x_{0:t} - x^i_{0:t}\big)dx_{0:t-1} \qquad (14)$$

where $x^i_{0:t}$ is the state trajectory and $y_{1:t}$ are the measurements up to time t. The simplest implementation of this algorithm, the Sequential Importance Re-sampling (SIR) particle filter, updates the weights using the likelihood of y_t as

$$w_t = w_{t-1}p(y_t|x_t) \qquad (15)$$

Long-term predictions are used to estimate the probability of failure in a system given a hazard zone that is defined via a probability density function with lower and upper bounds for the domain of the random variable, denoted as H_{lb} and H_{up}, respectively. The probability of failure at any future time instant is estimated by combining both the weights $w^{(i)}_{t+k}$ of predicted trajectories and specifications for the hazard zone through the application of the Law of Total Probabilities. The resulting RUL pdf, where t_{RUL} refers to RUL, provides the basis for the generation of confidence intervals and expectations for prognosis,

$$\hat{p}_{t_{RUL}} = \sum_{i=1}^{n} p\big(\text{Failure}|X = \hat{x}^{(i)}_{t_{RUL}}, H_{lb}, H_{up}\big) \qquad (16)$$

These novel diagnostic and prognostic technologies have been applied to a variety of systems ranging from ground vehicles to rotorcraft, UAVs, and other industrial/military application domains.

7.2. Model tuning

The parameters in the non-linear mappings $f(t)$ and $h_x(x(t))$ describe efficiently the system state whatever the environmental conditions or the external disturbances are. In this particular case, the function associating the fault rate to the operating time depends heavily on external conditions, such as temperature or corrosive agents, that may critically accelerate the degradation process (Nandi and others, 2005). In order to bring the model behavior closer to the real system, prediction is performed through a third time-dependent tunable model, following an approach similar to that described in (He, Li, Vachtsevanos, 2015). Again making use of symbolic regression powered by Eureqa software, it is possible to obtain a model linking the feature under analysis to operating time:

$$f^1_i(t) = 5.94 + 1.57 \cdot 10^{-8}t^2 + 6.47 \cdot 10^{-10}e^{Dt} \qquad (17)$$

The model parameter D is then tuned as more data is streaming in, following an iterative procedure featuring a recursive least square algorithm. Results of the fitting performed via Eureqa software for a possible degradation feature R^2 equal to 0.9964, mean squared error of 0.848A and mean absolute error of 1.432A.

7.3. RUL

The prediction algorithm makes use of 5000 particles and each prediction step is equal to a 4 hours' time interval. Prediction is terminated when all particles reach the threshold, set at 24 A, that is almost four times the average value for healthy conditions.

Taking advantage of the estimated end of life, t_{EOL}, for the electric motor, with t_p the prediction time, i.e. the instant at which the RUL prediction takes place, the RUL is computed as:

$$\text{RUL} = t_{EOL} - t_P \qquad (18)$$

A result example featuring a slow degradation is reported in Figure 10; the particles starts from an initial uniform distribution between 0 and 1 A. The algorithm quickly converges towards the real distribution, tracking the fault progression and providing the RUL estimate. The average RUL after fault detection for this case is equal to 415 flight hours. The value corresponding to a safety margin equal to 95% is 388 hours, while the required maintenance, corresponding to 95% rate of failures, is estimated at the latest in 509 hours.

7.4. Prognosis performance

The prognostic algorithm performance is evaluated through the metrics proposed by (Saxena, Celaya, Balaban, Goebel, Sasha & Schwabacher M, 2008) that are frequently adopted in the literature: the prognostic horizon H, the relative accuracy RA and the cumulative relative accuracy CRA.
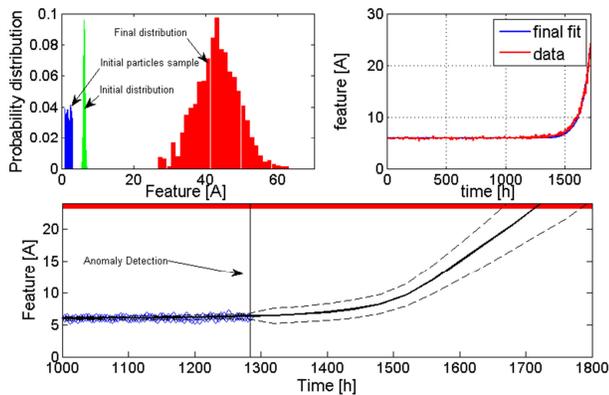
Figure 10. Prognosis results

The α–λ analysis has been used as well in order to visually display and verify that the RUL prediction remains (or not) inside the accuracy limit a for a generic time instant $t = t_D + \lambda(t_{EOL} - t_D)$, where t_D is the first prediction time and λ a scale factor ranging between 0 and 1.assess in the best possible way the system performance. The prognostic horizon H is derived through the same α–λ analysis by setting the accuracy limit equal to 20% of the RUL. Its average value over the considered datasets is 243 flight hours. The relative accuracy, a measure of the algorithm's capability to estimate precisely the RUL at a generic time instant t, is equal to 83.96% and the cumulative relative accuracy is 87.13%.

Repeated evaluation procedures confirm that the performance metrics remain within acceptable bounds and the prognosis performance is stable over every data set considered, consistently achieving an RCA value higher than 80% for λ higher than 0.2.

8. CONCLUSIONS

The most significant fault for an electric motor employed in EMAs for primary flight control has been assessed through the analysis of FMECA results. A novel set of pre-flight commands able to excite the system while enhancing the fault features and reducing the possible external disturbances has been proposed and discussed. A non-linear model has been built in order to study the effects of the TTS fault growth and extract a feasible feature, chosen among a few possible candidates based on performance metrics. A particle-filtering framework for anomaly detection and prognosis featuring a self-tuning non-linear model has been developed and employed. The system has proven to be precise and robust, achieving consistent performance for several initial data sets.

REFERENCES

Arulampalam S., Maskell S., Gordon, Clapp N. J.(2002) A Tutorial on Particle Filters for On-line Non-linear/Non-Gaussian Bayesian Tracking, *IEEE Trans. on Signal Processing*, Vol. 50 (2) pp. 174-188.

Balaban E., Saxena A, Goebel K., Byington C.S., Watson M., Bharadwaj S., Smith M. (2009) Experimental data collection and modeling for nominal and fault conditions on electro-mechanical actuators, *Annual Conference of the Prognostics and Health Management Society*, September 27-October 1, San Diego, CA.

Balaban E., Saxena A., Narasimhan S., Roychoudhury I., Gobel K., Koopmans M. (2010) Airborne electro-mechanical actuator test stand for development of prognostic health management systems, *Annual Conference of the Prognostics and Health Management Society*, October 10-16, Portland, Oregon.

Belmonte D., Dalla Vedova M.D.L., Maggiore P. (2015) New prognostic method based on spectral analysis techniques dealing with motor static eccentricity for aerospace electromechanical actuators, WSEAS Transactions on Systems, Vol. 14.

Brown D., Abbas M., Ginart A., Ali I., Kalgren P., Vachtsevanos G. (2010) Turn-off time as a precursor for gate bipolar transistor latch-up faults in electric motor drives, *Annual Conference of the Prognostics and Health Management Society*, October 10-16, Portland, Oregon.

Brown D.W., Georgoulas G., Bole B., Pei H.L., Orchard M., Tang L., Saha B., Saxena A., Goebel K., Vachtsevanos G. (2009) Prognostics enhanced reconfigurable control of electro-mechanical actuators, *Annual Conference of the Prognostics and Health Management Society*, September 27-October 1, San Diego, CA.

Christmann M., Seemann S. & Janker P. (2010). Innovative approaches to electromechanical flight control actuators and system, *Recent Advances in Aerospace Actuation Systems and Components*, May 5-7, Touluse, France.

Derrien J., Tieys P.,Senegas D. & Todeschi M. (2011). EMA Aileron COVADIS development. *SAE Technical paper*, 2011-01-2729.

Gokdere L.U., Bogdanov A., Chiu S. L., Keller K. J. & Vian J. (2006) Adaptive control of actuator lifetime, IEEE Aerospace Conference, March 4-11.

Hanselman D. (2006) Brushless Permanent Magnet Design, UK, Magna Physics.

He C., Li J., Vachtsevanos G.J (2015) Prognostics and health management of an automated machining process, *Mathematical Problems in Engineering*, 2015.

Jacazio G., Maggiore P., Della Vedova M., Sorli M. (2010) Identification of precursors of servovalves failures for implementation of an effective prognostics, *Proceedings of the 4th International Conference on Recent Advances in Aerospace Actuation Systems and Components*, May 5th-7th, Toulouse, France.

Jensen, S.C., Jenney G.D. & Dawson D. (2000). Flight test experience with an electromechanical actuator on the

F18 system research aircraft, *19th Digital Avionics System Conference* (page numbers), Edward, CA. doi: 10.1109/DASC.2000.886914.

Lessmeier C., Enge-Rosenblatt O., Bayer C., Zimmes D. (2014) Data acquisition and signal analysis from measured motor currents for defect detection in electromechanical drive systems, *European Conference of the Prognostics and Health Management Society*, July 8-10, Nantes, France.

Li H., Ye X., Chen C., Vachtsevanos G. (2014) A framework for model-based diagnostics and prognostics of switched-mode power supplies, Annual Conference of the Prognostics and Health Management Society, September 29 – October 2, Fort Worth, Texas.

Mohan N. (2003), First Course on Power Electronics and Drive, Minnessota, MNPERE.

Nandi S., Toliyat H.A.& Li X. (2005) Condition monitoring and fault diagnosis of electrical motors – a review, IEEE Transactions on Energy Conversion, Vol. 20, No.4.

Nordin M., Gallic J., Gutman P.O. (1997), New models for backlash and gear play, *International Journal od Adaptive Control and Signal Processing*, Vol. 11, pp. 49-63.

Orchard M (2007) *A Particle Filtering-based Framework for On-line Fault Diagnosis and Failure Prognosis*, PhD thesis, School of Electrical and Computer Engineering, Georgia Institute of Technology, Atlanta, GA..

Pratt, R, (2000). *Flight control systems: practical issues in design and implementation,* U.K.: IET.

Recksieck, M. (2012). Advanced high-lift system architecture with distributed electrical flap, *2nd International Workshop on Aircraft System Technologies*, March 29-30, Hamburg, Germany.

Roemer, M.J., & Tang, L. (2015). Integrated vehicle health and fault contingency management for UAVs. In Valavanis K.P., Vachtsevanos G.J., *Handbook of Unmanned Aerial Vehicles* (pages of chapter). Netherlands: Springer.

Saxena A., Celaya J., Balaban E., Goebel K, Sasha B. & Schwabacher M. (2008) Metrics for evaluating performance of prognostic techniques, *International Conference on Prognostics and Health Management*, October 6th-9th, Denver, CO.

Vachtsevanos G.J., Lewis F.L., Roemer M., Hess A., Wu B. (2006) *Intelligent Fault Diagnosis and Prognosis for Engineering Systems*, NY, John Wiley & Sons.

Wang L., Maré J.C., Fu Y. (2012) Investigation in the dynamic force equalization of dissimilar redundant actuation systems operating in active/active mode, 28th International Congress of the Aeronautical Sciences, Toulouse.